CIVIL ENGINEERING JOURNAL

Article no. 10

THE CIVIL ENGINEERING JOURNAL 1-2026

FINITE ELEMENT ANALYSIS OF BONDED PRESTRESSED STRENGTHENED HOLLOW SLAB BEAMS

Xilong Zheng

School of Intelligent and Architectural Engineering, Harbin University, No.109 Zhongxing Road, Harbin, Heilongjiang Province, China; Zhengxilong88@163.com

Received: 28.05.2025

Received in revised form: 21.01.2026

Accepted: 19.03.2026

ABSTRACT

With the continuous increase in traffic loads, the insufficient bearing capacity of existing bridges has become increasingly prominent, necessitating effective strengthening technologies to enhance their performance. This study focuses on bonded prestressed strengthened hollow slab beams. A finite element analysis method was employed to establish a discrete model comprising concrete (SOLID65 elements), composite mortar (SHELL41 elements), and prestressed tendons (LINK8 elements), with nonlinear spring elements used to simulate the interaction at the bonding layer. A three-point loading method was adopted to analyze the stress distribution characteristics of the strengthened beam under 10 kN and 80 kN loads, with emphasis on the stress responses in the anchorage zone, mid-span cross-section, and reinforcement. The results indicate significant stress concentration in the anchorage zone, requiring reinforcement in engineering design. When the cross-section approaches the destressed state (stress range: 0.1 MPa to -0.2 MPa), there is a notable discrepancy between finite element simulation results and material mechanics theoretical values. However, good agreement is observed in non-destressed states. Additionally, the stress variation trend of prestressed tendons under increasing loads aligns with theoretical predictions, with an error margin below 0.8%. This research provides theoretical and numerical references for the engineering application of bonded prestressed strengthening techniques.

KEYWORDS

Bonded prestressing, Hollow slab beams, Finite element analysis, Stress distribution, Strengthening technology, ANSYS simulation

INTRODUCTION

With rapid socio-economic development and improved living standards, vehicle load capacities and traffic volumes have significantly increased, leading to substantial increases in highway bridge loads [1,2]. However, bridges constructed in China's early years have low bearing capacities due to technological limitations, and prolonged use has exacerbated their deterioration [3]. In recent years, even newly constructed bridges have exhibited varying degrees of damage after years of operation, severely impacting transportation and economic development [4,5]. Therefore,

strengthening damaged bridges to enhance their load-bearing capacities is crucial for maintaining their functionality.

Section enlargement is a common bridge strengthening method. It involves removing damaged or loose parts of the structure and recasting concrete to expand the compression zone, thereby improving bending resistance, crack resistance, and stiffness [6-8]. While this method minimizes traffic disruption by working beneath the bridge, it faces constraints in special geographical or structural conditions, leading to increased costs, prolonged construction periods, and traffic impacts. Moreover, enlarging the section increases structural self-weight, potentially reducing load-bearing capacity [9-12].

Externally bonded reinforcement methods, such as attaching steel plates or high-strength materials (e.g., carbon fiber) to the surfaces of bridge components, enhance load-bearing capacity with minimal weight impact. These methods improve bending performance, control crack propagation, and enhance durability. However, issues like stress lag and adhesive quality limitations restrict their applicability [13-17].

Active strengthening techniques, such as prestressing, effectively utilize materials and mitigate strain lag effects inherent in passive methods [18-21]. Bonded prestressed composite mortar steel strand systems offer advantages such as convenient tensioning, simple anchorage, and high durability, making them widely recognized in engineering. While experimental studies on bonded prestressed hollow slab beams exist, finite element simulations remain limited. This study conducts a full-scale finite element simulation of a hollow slab beam to analyze stress distributions under varying loads and compares results with material mechanics theoretical values.

FINITE ELEMENT MODEL ESTABLISHMENT

An 8-meter full-scale beam model was simulated based on actual engineering parameters (Figure 1), incorporating eight prestressed steel strands. A discrete model was established using constraint equations. Schematic diagram of the anchoring system for hollow plate reinforcement is shown in Figure 2.

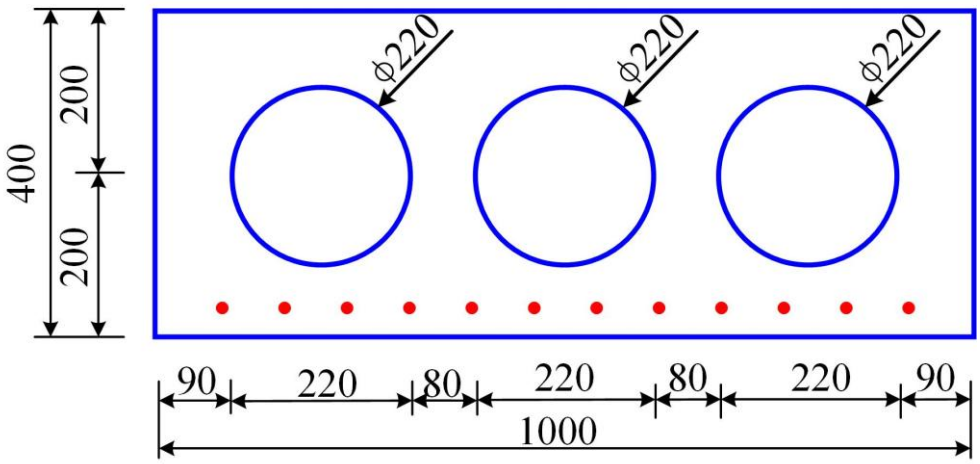

Fig. 1 - Cross-sectional Schematic of the 8 m Hollow Slab Beam (mm)

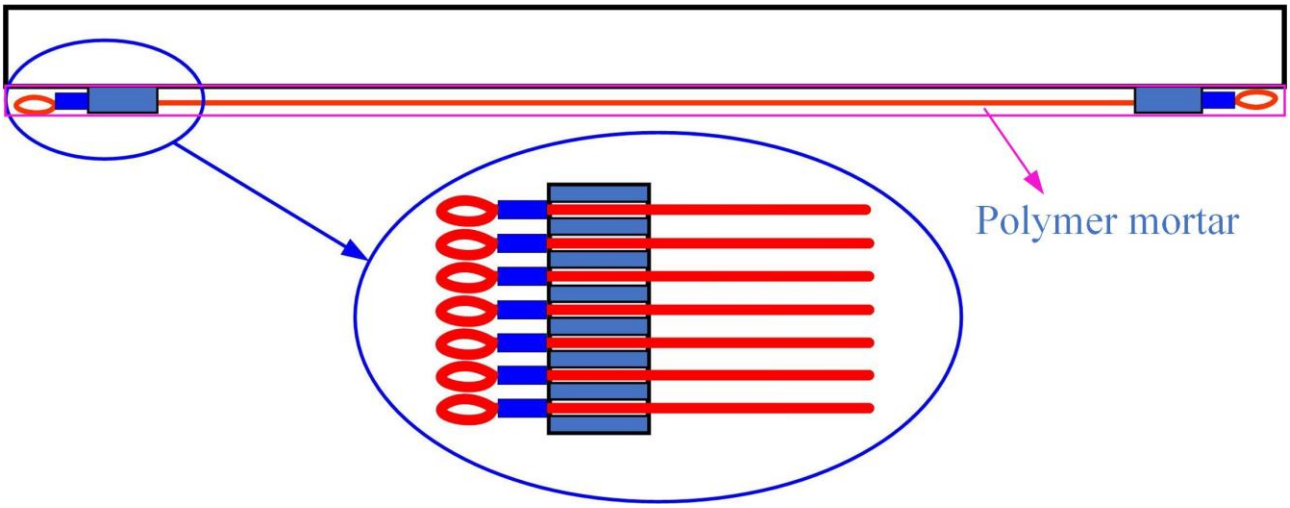

Fig. 2 - Schematic Diagram of the Anchoring System for Hollow Slab Reinforcement

Concrete was modelled using SOLID65 elements, composite mortar with SHELL41 elements, and reinforcement/prestressed tendons with LINK8 elements. In ANSYS, beam and truss elements are represented by two-node lines, requiring manual input of cross-sectional properties (e.g., area, inertia). The standard value of the compressive strength of concrete is 40 MPa.

The yield strength of ordinary steel bars is 335 MPa, and their elastic modulus is 200 GPa steel wire ropes with a moderate diameter of 4 mm were selected, offering high strength, low creep rate, and adequate ductility. The ropes possess a cross-sectional area of 10.55 mm², an ultimate tensile stress of 1200 MPa, an ultimate tensile strain of 0.02, and an elastic modulus of 130 GPa.

Meshing for composite mortar and concrete utilized element sizes of approximately 50 mm × 50 mm × 125 mm. The finite element model is shown in Figures 3–4. Full displacement compatibility between reinforcement and concrete was assumed, neglecting slippage.

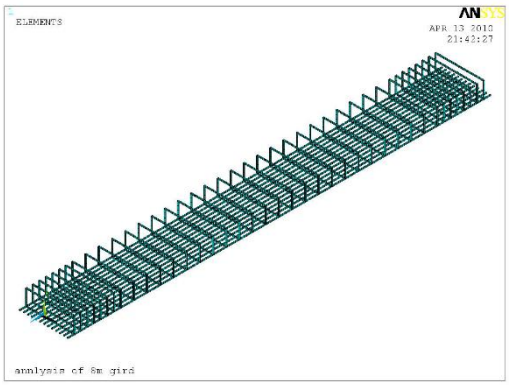

Fig. 3 - Reinforcement Simulation

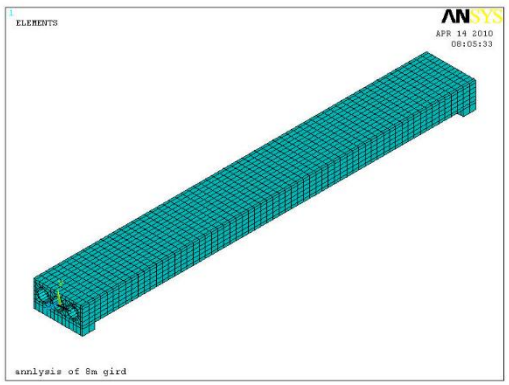

Fig. 4 - Meshing Results

Composite mortar-concrete interaction was modelled using nonlinear spring elements (CONBIN39) in three directions: normal (perpendicular to the interface), longitudinal shear (parallel to beam length), and transverse shear (perpendicular to beam length) (Figures 5–6). To achieve pure bending at mid-span, three-point loading was applied at 2.5 m from the supports. Surface loads and support pads were used to improve convergence.

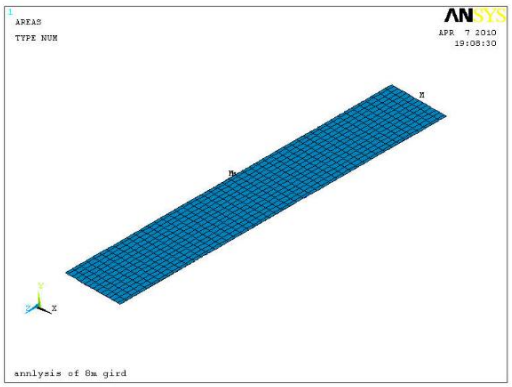

Fig. 5 - Composite Mortar Simulation

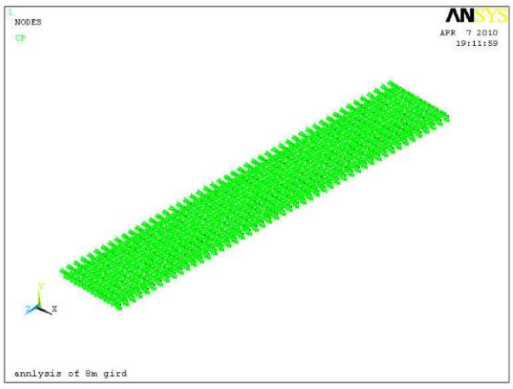

Fig. 6 - Spring Element Simulation

STRESS ANALYSIS UNDER THREE-POINT LOADING

Post-processing extracted displacements, stresses, strains, and deformations. Stress analyses under 10 kN and 80 kN loads (excluding self-weight) are detailed below.

Stress Analysis Under 10 kN Load

1) Global Stress Distribution

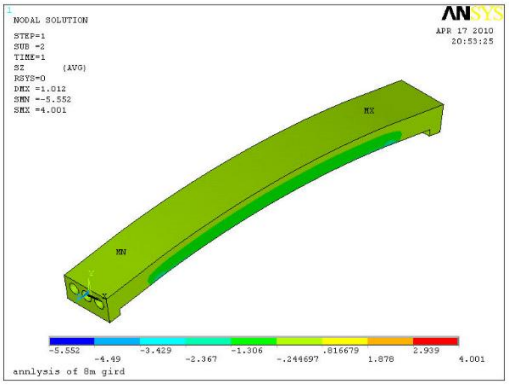

Fig. 7 - Global Equivalent Stress Contour (MPa)

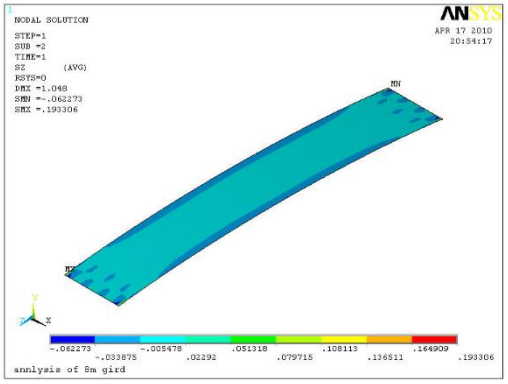

Fig. 8 - Composite Mortar Equivalent Stress Contour (MPa)

Maximum tensile stress (4.00 MPa) occurred at the bottom anchorage zone, while minimum stress (5.55 MPa) appeared near the top at 1/3 span from supports. Stress concentration in the anchorage zone necessitates localized reinforcement.

2) Cross-Sectional Stress Analysis

Z-direction stress contours at 1/8, 1/4, 3/8, and mid-span sections are shown in Figures 8–11. Under 10 kN, tensile stresses (0.17–0.24 MPa) increased toward mid-span, while compressive stresses (0.66–1.29 MPa) dominated the bottom. Complex stresses were observed at 1/8 span due to anchorage effects.

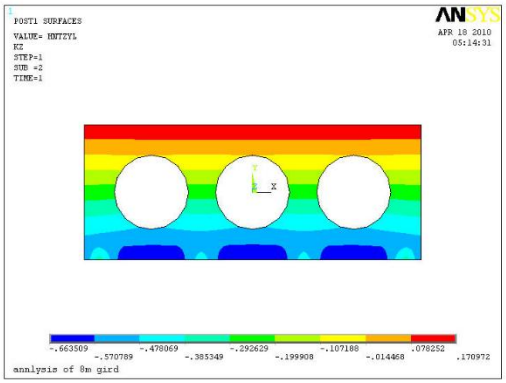

Fig. 9 - 1/8 Section Z-Direction Stress Contour (MPa)

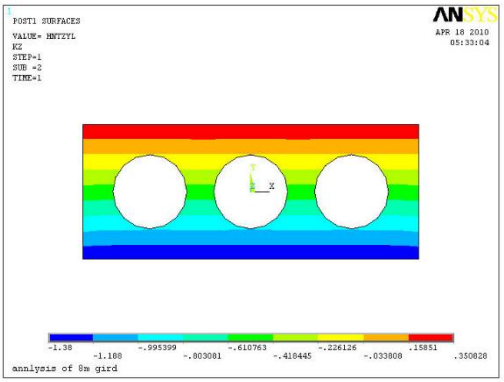

Fig. 10 - 2/8 Section Z-Direction Stress Contour (MPa)

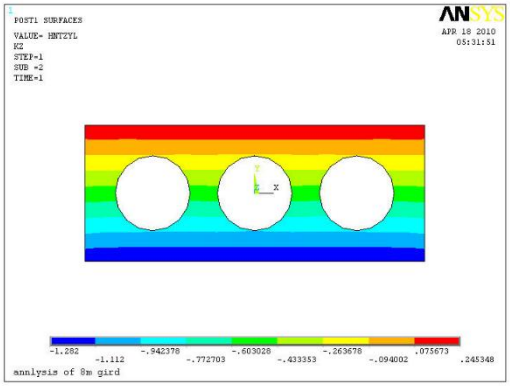

Fig. 11 - 3/8 Section Z-Direction Stress Contour (MPa)

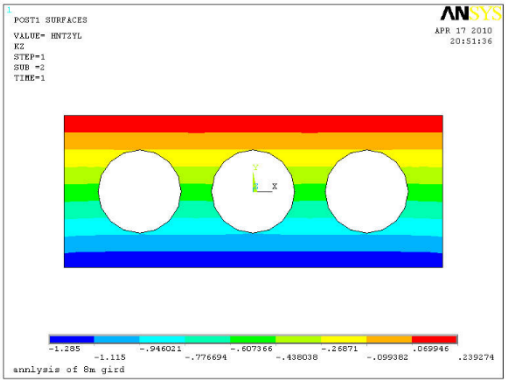

Fig. 12 - Mid-Span Section Z-Direction Stress Contour (MPa)

In ANSYS, the system defaults to tensile stress as positive and compressive stress as negative. As shown in Figures 9-12, under a total load of 10 kN (excluding beam dead load), the sections from the 1/8-span to mid-span exhibit tensile stress, varying from 0.17 MPa to 0.24 MPa. Conversely, the beam bottom sections show compressive stress, ranging from 0.66 MPa to 1.29 MPa. At the 1/8-span section, stress distribution is more complex due to the anchor device effect.

3) Main Reinforcement Stress Analysis

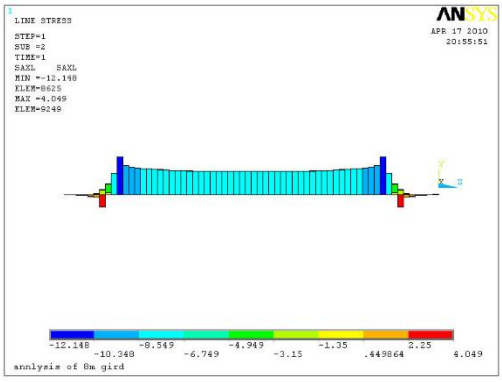

(a) Ordinary Reinforcement Stress Diagram

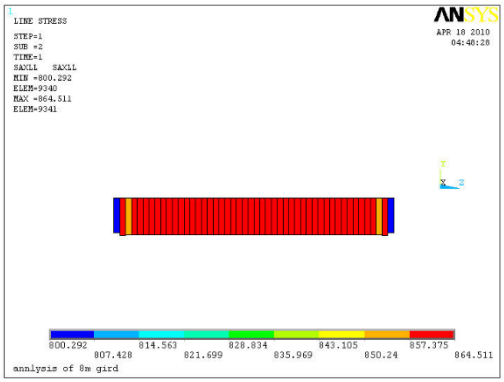

(b) Prestressed Reinforcement Stress Diagram

Fig. 13 - Stress Contour of Internal Reinforcement in Post-Strengthened Beam (MPa)

Figure 13 illustrates the stress contour of internal reinforcement in a post-strengthened beam under a concentrated load of 10 kN. As shown in the diagram, the maximum stress of ordinary reinforcement occurs in the mid-span region, reaching 5.76 MPa under tension. Conversely, the minimum stress of ordinary reinforcement, measured at 12.15 MPa under compression, appears between the concentrated force application point and the support. Additionally, the stress of prestressed reinforcement in the mid-span region is recorded as 864.51 MPa.

Stress Effect Analysis of the Beam Under 80 kN Load Application

1) Integral Beam Stress Analysis

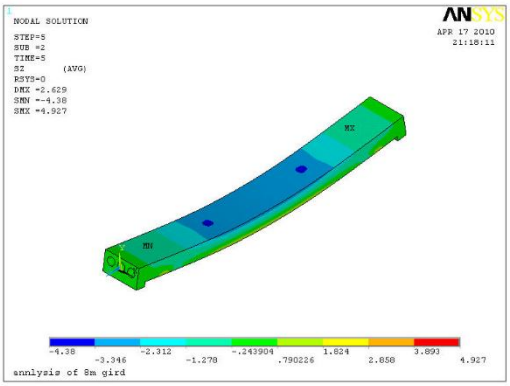

Fig. 14 - Integral Beam Equivalent Stress Contour (MPa)

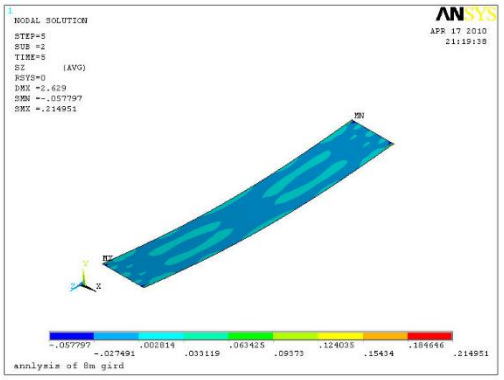

Fig. 15 - Composite Mortar Equivalent Stress Contour (MPa)

As shown in Figure 14, under the applied load, the integral beam exhibits maximum tensile stress (4.93 MPa) at the bottom anchorage region and maximum compressive stress (4.38 MPa) at the top slab, located 1/3 span away from the support. The primary cause of the maximum tensile stress is excessive local stress concentration at the anchorage point. Figure 15 presents the equivalent stress contour of composite mortar, where maximum tensile stress also appears in the anchorage region. This indicates that the anchorage zone is a structural weakness requiring localized reinforcement design in engineering strengthening.

2) Main Beam Stress Analysis at Calculated Sections

Z-direction stress contours were extracted for the 1/8-span, 2/8-span, 3/8-span, and mid-span sections of the main beam, as illustrated in Figures 15-18.

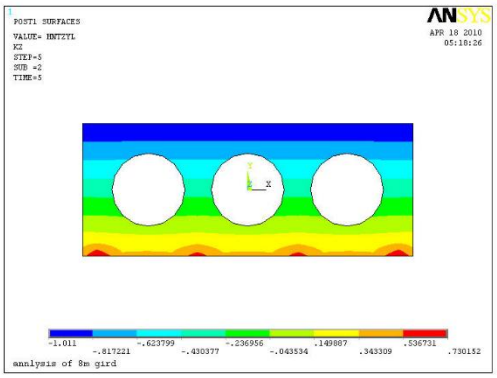

Fig. 16 - Z-Direction Stress Contour of the 1/8-Span Section (MPa)

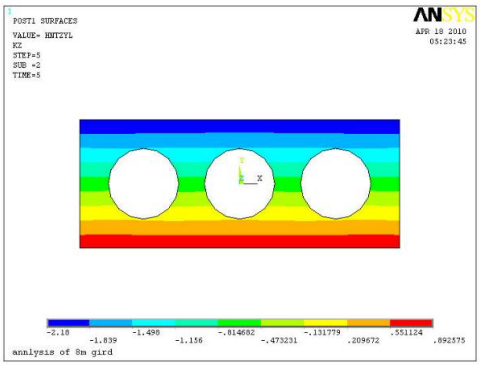

Fig. 17 - Z-Direction Stress Contour of the 2/8-Span Section (MPa)

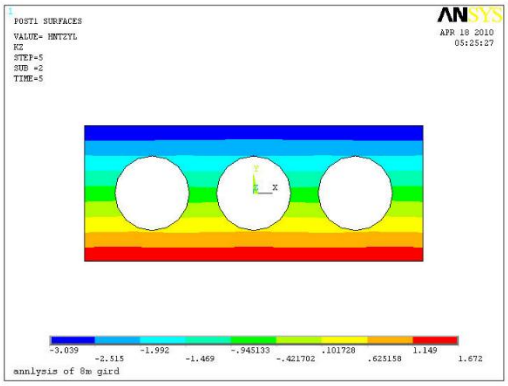

Fig. 18 - Z-Direction Stress Contour of the 3/8-Span Section (MPa)

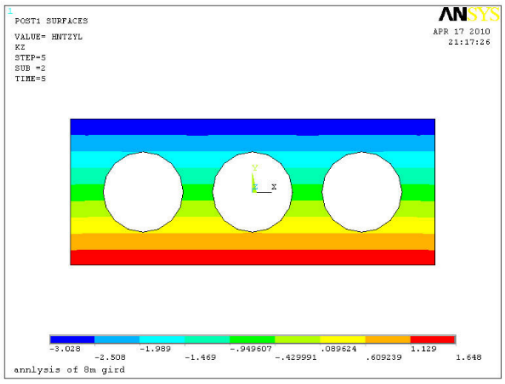

Fig. 19 - Z-Direction Stress Contour of the Mid-Span Section (MPa)

In ANSYS, tensile stress is defined as positive by default, while compressive stress is negative. As observed in Figures 16-19, under a total load of 80 kN, compressive stresses (excluding self-weight and dead loads of the main beam) are observed across sections from the 1/8-span to mid-span, ranging from 1.01 MPa to 3.03 MPa. Tensile stresses are observed at the beam bottom sections, ranging from 0.73 MPa to 1.65 MPa. At the 1/8-span section, stress distribution is more complex due to the influence of anchorage devices.3) Main Reinforcement Stress Analysis

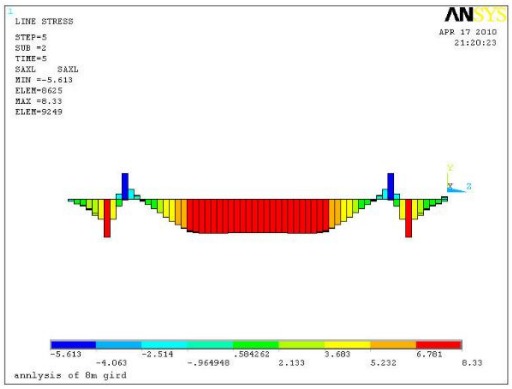

(a) Stress Contour of Ordinary Reinforcement

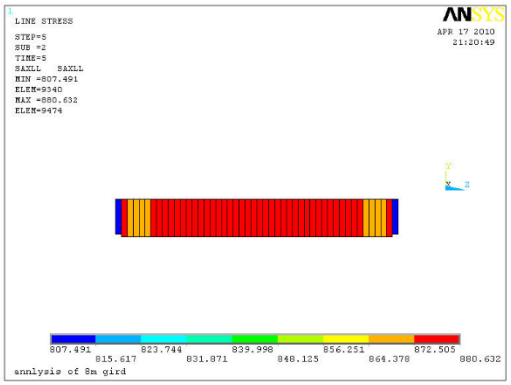

(b) Stress Contour of Prestressed Reinforcement

Fig. 20 - Stress Contour of Internal Reinforcement in Post-Strengthened Beam (MPa)

Figure 20 illustrates the internal reinforcement stress distribution in the post-strengthened beam under an 80 kN concentrated load. As shown in the figure, the maximum tensile stress of ordinary reinforcement occurs in the mid-span region, reaching 8.33 MPa, while the minimum compressive stress (5.61 MPa) is observed in the 1/8-span region. The prestressed reinforcement at mid-span exhibits a stress level of 880.63 MPa.

COMPARATIVE ANALYSIS BETWEEN ANSYS-CALCULATED VALUES AND THEORETICAL SOLUTIONS FROM MECHANICS OF MATERIALS

To validate the accuracy of numerical simulations, stress values calculated via solid element simulations at the mid-span section were compared with analytical results derived from mechanics of materials under applied loads of 10 kN, 20 kN, 40 kN, 60 kN, and 80 kN. Detailed computational data are provided in Table 1 and Table 2.

Tab. 1 - Post-Strengthened Beam Concrete Stress Calculation Results (MPa)

Load kN	Calculated Section Top Edge Stress				Calculated Section Bottom Edge Stress			
	Theoretical Value from Mechanics of Materials	Solid Element Simulation Value	Difference Between Simulation and Theory	Percentage Difference (%)	Theoretical Value from Mechanics of Materials	Solid Element Simulation Value	Difference Between Simulation and Theory	Percentage Difference (%)
10	-0.30	-0.24	0.06	19.8	1.35	1.29	-0.06	4.7
20	0.19	0.23	0.04	22.7	0.92	0.87	-0.05	5.7
40	1.13	1.16	0.03	2.8	0.08	0.03	-0.05	66.3
60	2.09	2.10	0.01	0.2	-0.76	-0.81	-0.05	6.6
80	3.05	3.03	-0.02	0.7	-1.61	-1.65	-0.04	2.4

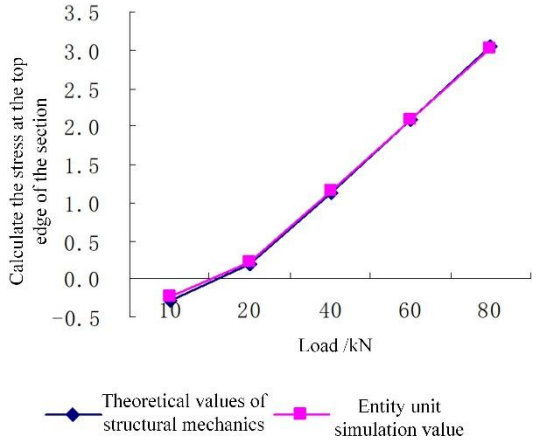

Fig. 21 - Post-Strengthened Beam Top Edge Stress Under Varying Load Levels

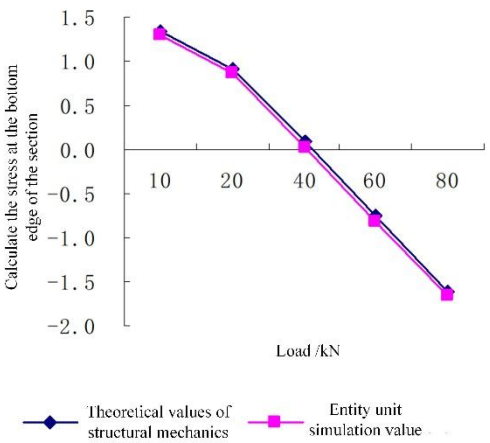

Fig. 22 - Post-Strengthened Beam Bottom Edge Stress Under Varying Load Levels

Figures 21 and 22 depict the top/bottom edge stresses at the mid-span section of the post-strengthened beam under varying load levels. As shown, discrepancies exist between solid element simulation results and theoretical solutions from mechanics of materials, with the magnitude of differences progressively decreasing as load intensity increases. This phenomenon primarily arises from the inherent assumptions embedded in classical mechanics of materials theories, such as the plane section assumption and homogeneous material assumption, which derive sectional stresses through inverse calculation of member bending moments. In contrast, solid element simulations adhere to finite element principles by directly capturing internal force distributions at discrete locations through structural behavior modeling. Consequently, theoretical deviations are inevitable between these two methodologies. The application of solid element modeling enables refined structural analysis by accounting for localized stress variations and complex geometric/material interactions.

Tab. 2 - Post-Strengthened Beam Reinforcement Stress Calculation Results (MPa)

Load kN	Calculated Section Top Edge Stress				Calculated Section Bottom Edge Stress			
	Theoretical Value from Mechanics of Materials (MPa)	Solid Element Simulation Value (MPa)	Difference Between Simulation and Theory (MPa)	Percentage Difference (%)	Theoretical Value from Mechanics of Materials (MPa)	Solid Element Simulation Value (MPa)	Difference Between Simulation and Theory (MPa)	Percentage Difference (%)
10	6.00	5.76	-0.24	4.0%	-863.09	-864.51	-1.423	0.2%
20	3.49	3.27	-0.22	6.3%	-866.58	-865.76	0.814	0.1%
40	-0.08	-0.13	-0.05	62.5%	-873.55	-869.05	4.504	0.5%
60	-4.88	-5.08	-0.20	4.0%	-880.53	-874.84	5.689	0.6%
80	-10.84	-11.08	-0.24	2.2%	-887.50	-880.63	6.868	0.8%

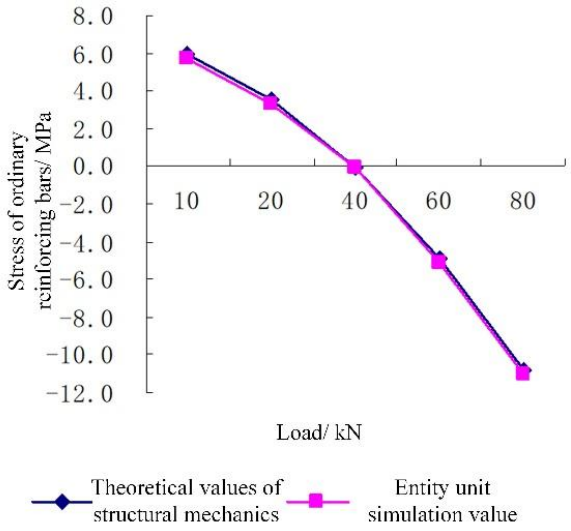

Fig. 23 - Post-Strengthened Beam Ordinary Reinforcement Stress Under Varying Load Levels

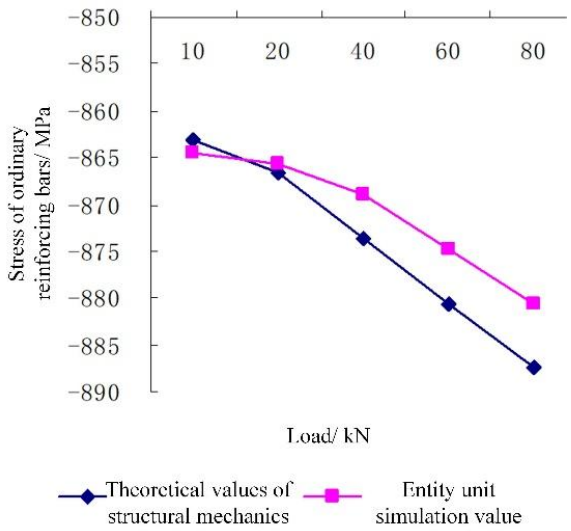

Fig. 24 - Post-Strengthened Beam Prestressed Reinforcement Stress Under Varying Load Levels

Figures 23 and 24 illustrate the stress variations of ordinary reinforcement and prestressed reinforcement, respectively, in the post-strengthened beam under varying load levels. Observations reveal that at lower load magnitudes, the discrepancy between solid element simulation results and theoretical values from mechanics of materials for ordinary reinforcement remains relatively small. However, as load intensity increases, the deviation for prestressed reinforcement stress exhibits a progressive growth trend, though the percentage difference remains minimal (0.1%–0.8%).

Correlation analysis with Table 1 and Table 2 data reveals notable discrepancies between calculation methods under specific loading conditions. At 20 kN total load, the mid-span top edge concrete compressive stress exhibits significant variation: 0.185 MPa (theoretical) vs. 0.23 MPa (simulation). Similarly, at 40 kN total load, the mid-span ordinary reinforcement tensile stress shows marked divergence: 0.08 MPa (theoretical) vs. 0.13 MPa (simulation). These phenomena stem from the beam's stress state transition: at 20 kN, the top edge approaches stress neutralization (zero stress), while at 40 kN, the bottom edge enters stress neutralization. Consequently, when sectional stresses range between 0.1 MPa (tension) and -0.2 MPa (compression) during stress neutralization transitions, the two calculation methodologies produce pronounced discrepancies due to the complexity of stress redistribution. Conversely, when sectional stresses are from the neutralization state (i.e., at higher stress magnitudes), both calculation methods demonstrate consistent results.

COMPARATIVE ANALYSIS OF FINITE ELEMENTS BEFORE AND AFTER REINFORCEMENT

In order to clearly understand the improvement effect of the beam reinforced with bonded prestress, studies were conducted on the unreinforced beam, the beam reinforced with 8 prestressed steel strands, and the beam reinforced with 12 prestressed steel strands. The mid-span section was simulated using solid elements and the calculated values were compared with the theoretical values based on material mechanics under loads of 10kN, 20kN, 40kN, 60kN, and 80kN. The specific calculation values are shown in Tables 3 and 4. The top edge concrete stress and bottom edge steel bar stress before and after reinforcement are shown in Figures 25 and 26.

Tab. 3 - Top Edge Stress Results Before and After Reinforcement (MPa)

Load kN	Calculated Section Top Edge Stress				
	Unstrengthened	Strengthened with 8 prestressed steel strands	Percentage Difference (%)	Strengthened with 12 prestressed steel strands	Percentage Difference (%)
10	0.57	-0.24	-141.9%	-0.87	-253.2%
20	1.36	0.23	-83.3%	-0.12	-109.0%
40	2.54	1.16	-54.3%	0.88	-65.4%
60	2.97	2.10	-29.5%	1.56	-47.4%
80	4.32	3.03	-29.9%	2.20	-49.2%

Tab. 4 - Steel Bar Stress Results Before and After Reinforcement (MPa)

Load kN	Calculated Steel Bar Stress				
	Unstrengthened	Strengthened with 8 prestressed steel strands	Percentage Difference (%)	Strengthened with 12 prestressed steel strands	Percentage Difference (%)
10	-1.02	5.76	-664.7%	6.25	-712.8%
20	-4.37	3.27	-174.8%	5.37	-222.9%
40	-6.28	-0.13	-97.9%	2.64	-142.1%
60	-14.36	-5.08	-64.6%	-1.73	-88.0%
80	-22.59	-11.08	-51.0%	-5.65	-75.0%

From Table 3 and Figure 25, it can be seen that when the load is 20kN, the compressive stress at the top edge of the 8 prestressed steel strand reinforced beam is 0.23 MPa, which is 83.3% lower than that of the un-reinforced beam, indicating that the application of prestress reduces the tensile stress generated at the top edge during the loading process and thereby lowers the top edge pressure. The tensile stress of the top edge concrete of the 12 prestressed steel strand reinforced beams is -0.12 MPa, indicating that with the increase in the number of prestressed steel strands, the tensile stress of the top edge concrete increases, but it is still under tension at this time. When the load is 80kN, the compressive stress of the 8 prestressed steel strand reinforced beams is 3.028MPa, which is 29.9% lower than the compressive stress of the top edge concrete of the un-reinforced beam. The compressive stress of the top edge concrete of the 12 prestressed steel strand reinforced beams is 19.3% lower than that of the 8 prestressed steel strand reinforced beams, indicating that with the increase in the number of prestressed steel strands, the compressive stress at the top edge decreases.

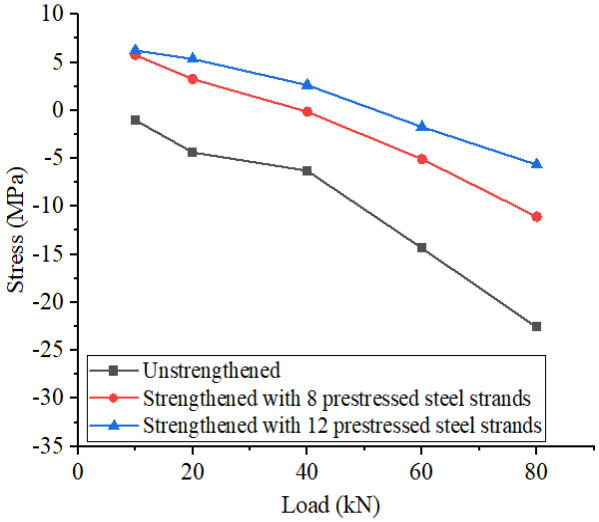

Fig. 25 - Stress of the top edge concrete under different loads

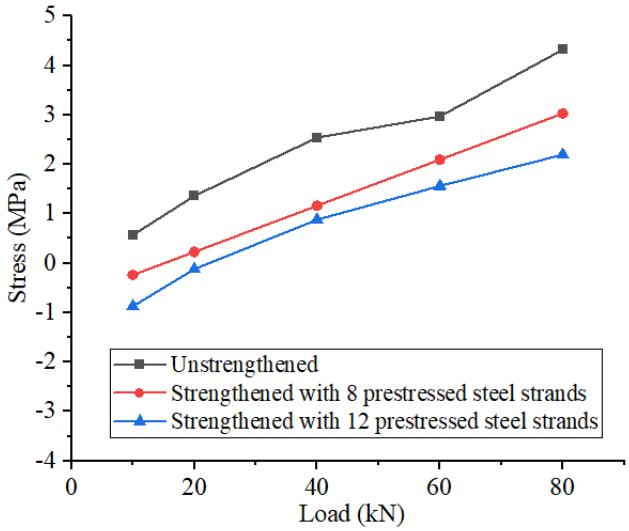

Fig. 26 - Stress of ordinary reinforcing bars under different loads

From Table 4 and Figure 26, it can be seen that when the load is 20 kN, the tensile stress of the unreinforced beam is -4.37 MPa, and the bottom edge compressive stress of the 8 prestressed steel strand reinforced beams is 3.27 MPa. This indicates that the application of prestress causes compressive stress at the bottom edge of the beam. The compressive stress of the bottom edge of the 12 prestressed steel strand reinforced beams is 48.1% higher than that of the 8 prestressed steel strand reinforced beams, indicating that as the number of prestressed steel strands increases, the compressive stress at the bottom edge increases. When the load is 80 kN, the tensile stress of the 8 prestressed steel strand reinforced beams' steel bars is -11.08 MPa, which is 51.0% lower than that of the unreinforced beam. The tensile stress of the bottom edge steel bars of the 12 prestressed steel strand reinforced beams is 24.0% lower than that of the 8 prestressed steel strand reinforced beams, indicating that as the number of prestressed steel strands increases, the compressive stress at the top edge decreases.

In order to clearly understand the improvement effect of the beam reinforced with bonded prestress, studies were conducted on the unreinforced beam, the beam reinforced with 8 prestressed steel strands, and the beam reinforced with 12 prestressed steel strands. The mid-span section was simulated using solid elements and the calculated values were compared with the theoretical values based on material mechanics under loads of 10kN, 20 kN, 40 kN, 60 kN, and 80 kN. The crack width before and after reinforcement are shown in Figures 25 and 26.

Tab. 5 - Crack Width Before and After Reinforcement (mm)

Load kN	Calculated Steel Bar Stress				
	Unstrengthen	Strengthened with 8 prestressed steel strands	Percentage Difference (%)	Strengthened with 12 prestressed steel strands	Percentage Difference (%)
10	0	0	/	0	/
20	0	0	/	0	/
40	0.03	0	-100%	0	-100%
60	0.07	0.02	-71.4%	0	-100%
80	0.15	0.06	-60.0%	0.04	-73.3%

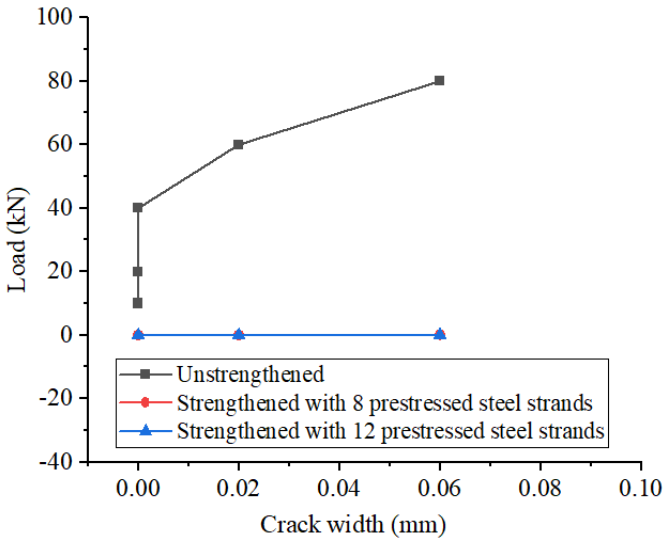

Fig. 27 – Crack width under different loads

From Table 5 and Figure 27, it can be seen that when the load is 20kN, Neither the reinforced beams nor the un-reinforced beams showed any cracks, indicating that the beams were still in the elastic working stage at this point. When the load is 40kN, the crack width of the unreinforced beam is 0.03mm, while the reinforced beam does not crack. When the load is 60kN, the crack width of the unreinforced beam is 0.07mm, and the crack width of the 8 prestressed steel strand reinforced beam is 0.02mm, while the 12 prestressed steel strand reinforced beams do not crack. When the load is 80kN, the crack width of the unreinforced beam is 0.15mm, the crack width of the 8 prestressed steel strand reinforced beam is 0.06mm, and the crack width of the 12 prestressed steel strand reinforced beam is 0.04mm, indicating that the prestressed steel strand reinforcement can effectively delay the appearance of cracks and limit the expansion of cracks.

STRESS ANALYSIS OF REINFORCED BEAMS

For components that have been reinforced by certain means, when considering the combined section bearing live loads, and fully taking into account the effect of the added reinforcing materials, the calculation of the section stress should still be based on the cracked section of the component.

The calculation of the section stress is to calculate the geometric characteristic values of the converted section of the combined section after reinforcement based on the cracked section, and then calculate according to the relevant formulas in material mechanics. Finally, the stress calculated at each stage needs to be superimposed to obtain the final result.

According to the force analysis, the concentrated load and the bending moment caused by the live load generated by the prestressed reinforcement will increase the compressive stress in the compression zone at the top of the original beam, while the bending moment generated by the prestressed reinforcement will reduce the compressive stress in the compression zone. The concentrated load and the bending moment generated by the prestressed reinforcement will reduce the tensile stress of the main reinforcement of the original beam, while the standard value of the bending moment caused by the live load will also reduce the tensile stress of the main reinforcement. Stress calculation diagram for the main section is shown in Figure 28. Strain calculation diagram for the main section under the ultimate state is shown in Figure 29.

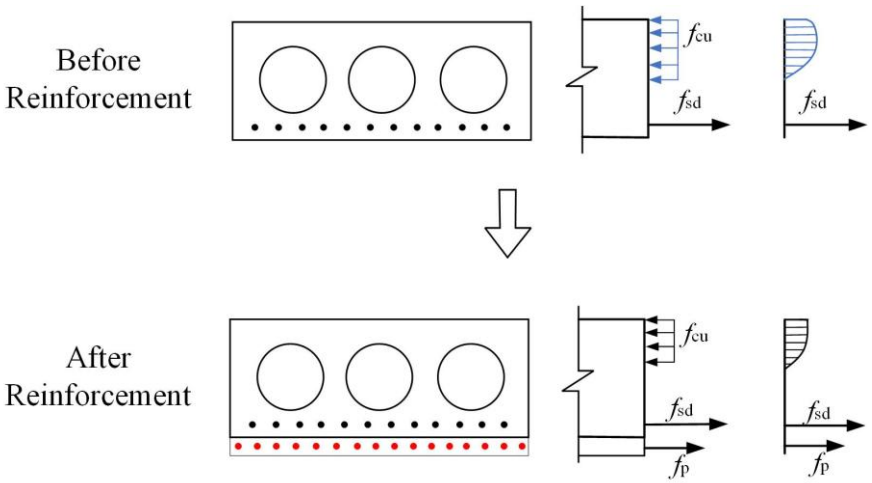

Fig. 28 – Stress calculation diagram for the main section

After the reinforcement of the beam with load, both the stress and strain will change. To simplify the calculation, the final strain is divided into two parts: before reinforcement and the ultimate state. ε_{c2} is taken as the strain increment of the concrete compression zone at the upper edge from before reinforcement to the ultimate state, and ε_{s2} is taken as the strain increment of the main reinforcement of the original beam from before reinforcement to the ultimate state. The stress calculation diagram of the reinforced beam under the ultimate state is shown below.

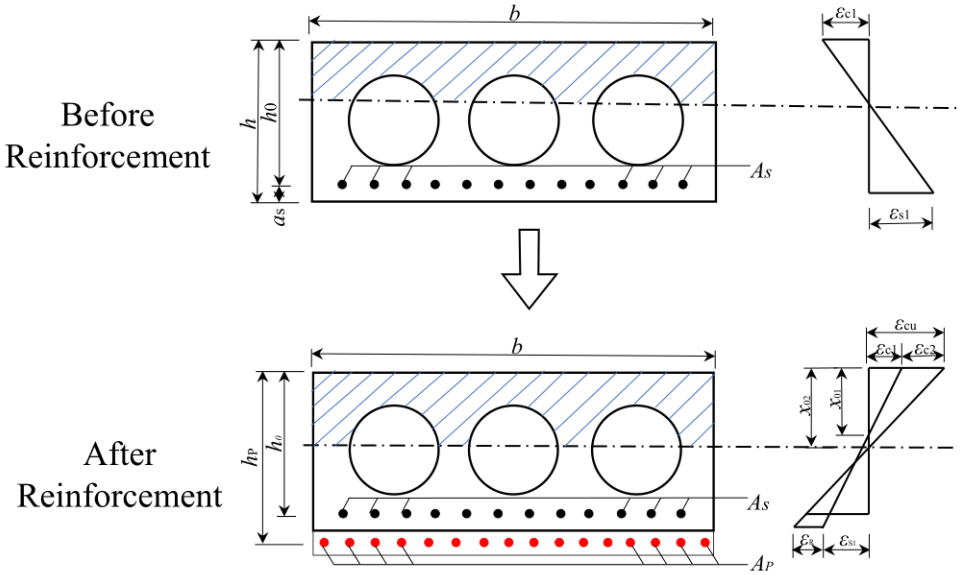

Fig. 29 Strain calculation diagram for the main section under the ultimate state:

$$\xi_b = \frac{\beta \varepsilon_{cu}}{\varepsilon_{s1} + \varepsilon_{s2} + \varepsilon_{cu}} \tag{1}$$

$$\varepsilon_{s2} = \frac{h_0}{h_p}\left(\varepsilon_R + \varepsilon_{c2}\right) - \varepsilon_{c2} \tag{2}$$

$$\varepsilon_R = \frac{\sigma_R - \sigma_{con}}{E_R} \tag{3}$$

In the formula:

ε_R — Strain after adding prestressed reinforcement;

σ_{con} — Control of prestressed reinforcement tensioning for controlling prestress;

σ_R — The stress of the post-installed reinforcement in the ultimate state;

E_R — The elastic modulus after adding reinforcing bars;

h_P — The distance from the combined action point of the prestressed reinforcing bars to the compressive edge of the section.

CONCLUSION

This paper introduces a numerical analysis methodology for finite element simulation of bonded prestressed reinforcement systems, analyzing the stress distribution in post-strengthened beams under varying load levels and comparing results with theoretical solutions from mechanics of materials. The key conclusions are summarized as follows:

(1) ANSYS enables accurate simulation of bonded prestressed reinforcement systems, particularly in beam end anchorage zones where complex stress states exist. Classical mechanics of materials theories often lack precision in such regions due to localized stress concentrations, necessitating the use of solid element modeling for detailed analysis at beam end sections.

(2) When the calculated section approaches stress neutralization (0.1 MPa tension to -0.2 MPa compression), significant discrepancies arise between finite element simulation results and theoretical predictions. This phenomenon stems from the complex stress redistribution occurring at sectional edges during neutralization transitions, where conventional theoretical assumptions fail to capture localized stress variations.

(3) At mid-span sections under non-neutralized stress states, solid element simulations and theoretical calculations demonstrate good agreement. For routine engineering design where sections operate away from neutralization conditions, classical mechanics of materials theories provide sufficiently accurate results with acceptable computational efficiency.

REFERENCE

[1] Li X, Wu G, Popal M S,. 2018. Experimental and numerical study of hollow core slabs strengthened with mounted steel bars and prestressed steel wire ropes. Construction and Building Materials, 2018, 188: 456-469. ISSN: 0950-0618, https://doi.org/10.1016/j.conbuildmat.2018.08.073

[2] Wang Z, Wang M, Xu Q,. 2021. Experimental research on prestressed concrete hollow-core slabs strengthened with externally bonded bamboo laminates. Engineering Structures, vol. 244, p. 112786. ISSN: 0141-0296, https://doi.org/10.1016/j.engstruct.2021.112786

[3] Yang J, Hou P, Pan Y,. 2021. Shear behaviors of hollow slab beam bridges strengthened with high-performance self-consolidating cementitious composites. Engineering Structures, vol. 242, p.112613. ISSN: 0141-0296, https://doi.org/10.1016/j.engstruct.2021.112613

[4] Yang J, Guo H, Yang C,. 2024. Experimental investigation and evaluation of shear performance of hollow slab beams strengthened by cavity grouting method. Case Studies in Construction Materials, vol. 20, p. e03184. ISSN: 2214-5095, https://doi.org/10.1016/j.cscm.2024.e03184

[5] Li X H, Wu G, Wang S,. 2019. Flexural behavior of hollow-core slabs strengthened with prestressed basalt FRP grids. Journal of Composites for Construction, vol. 23, n. 3, p. 04019016. ISSN: 1090-0268, https://doi.org/10.1016/j.cscm.2024.e03184

[6] Pachalla S K S, Prakash S S,. 2027. Load resistance and failure modes of GFRP composite strengthened hollow core slabs with openings. Materials and Structures, vol. 50, p. 1-14. ISSN: 1359-5997, https://doi.org/10.1617/s11527-016-0883-8

[7] Song S, Deng M, Zhang Y,. 2024. Effects of textile type on the flexural properties of prefabricated hollow-core slabs strengthened with PVA fibers-improved TRM. Journal of Building Engineering, vol. 87, p. 109103. ISSN: 2352-7102, https://doi.org/10.1016/j.jobe.2024.109103

[8] Zhang H, Huang W, Liu B,. 2022. Flexural behavior of precast concrete hollow-core slabs with high-strength tendons. Journal of Building Engineering, vol. 59, p. 105050. ISSN: 2352-7102, https://doi.org/10.1016/j.jobe.2022.105050

[9] Di J, Sun Y, Yu K,. 2020. Experimental investigation of shear performance of existing PC hollow slab. Engineering Structures, vol. 211, p. 110451. ISSN: 0141-0296, https://doi.org/10.1016/j.engstruct.2020.110451

[10] Chen X, Ma Q,. 2024. Experimental study on the flexural performance of concrete hollow composite slabs with tightly connected panel sides. Scientific Reports, vol. 14, n. 1, p. 20784. ISSN: 2045-2322, https://doi.org/10.1038/s41598-024-71880-8

[11] Elharouney O, Elkateb M, Khalil A,. 2021. Behaviour of prestressed hollow core slabs strengthened with NSM CFRP strips around openings: A finite element investigation. Engineering Structures,vol. 238, p. 112262. ISSN: 0141-0296, https://doi.org/10.1016/j.engstruct.2021.112262

[12] Badran H, Alkloub A,. 2025. Strengthening of precast pretensioned hollow core slabs exposed to fire. Journal of Structural Integrity and Maintenance, vol. 10, n. 1, p. 2471156. ISSN: 2470-5314, https://doi.org/10.1080/24705314.2025.2471156

[13] Zhang S, Du S, Ang Y,. 2021. Study on performance of prestressed concrete hollow slab beams reinforced by grouting with ultra-high performance concrete. Case Studies in Construction Materials, vol. 15, p. 83. ISSN: 2214-5095, https://doi.org/10.1016/j.cscm.2021.e00583

[14] Chen J, Li X, Zhu Q,. 2023. Experimental research on mechanical behavior and strengthening technologies of joints in hollow-core slab bridge. Structures, vol. 49, p. 223-239. ISSN: 2352-0124, https://doi.org/10.1016/j.istruc.2023.01.103

[15] Xun S, Shiping Y, Yuhou Y,. 2022. Comparative analysis of flexural performance of old full-scale hollow slab beams reinforced with fiber composites. Construction and Building Materials, vol. 338, p. 127657. ISSN: 0950-0618, https://doi.org/10.1016/j.conbuildmat.2022.127657

[16] Wang J, Jia Y, Zhang G,. 2018. Experimental study on prestressed concrete hollow slabs in service strengthened with prestressed CFRP plates. International Journal of Structural Integrity, vol. 9, n. 5, p. 587-602. ISSN: 1757-9864, https://doi.org/10.1108/IJSI-08-2017-0049

[17] Al-Rubaye M, Manalo A, Alajarmeh O,. 2020. Flexural behaviour of concrete slabs reinforced with GFRP bars and hollow composite reinforcing systems. Composite structures, vol. 236, p. 111836. ISSN: 0263-8223, https://doi.org/10.1016/j.compstruct.2019.111836

[18] Kankeri P, Prakash S S,. 2017. Efficient hybrid strengthening for precast hollow core slabs at low and high shear span to depth ratios. Composite structures, vol. 170, p. 202-214. ISSN: 0263-8223, https://doi.org/10.1016/j.compstruct.2017.03.034

[19] Yang L, Shen Q, Lu M,. 2025. Experimental Study on Bending Behaviors of Ultra-High-Performance Fiber-Reinforced Concrete Hollow-Core Slabs. Buildings, vol. 15, n. 5, p. 812. ISSN: 2075-5309, https://doi.org/10.3390/buildings15050812

[20] Xiao J L, Liu Y F, Feng H L,. 2025. Field tests and structural performance evaluation of existing reinforced concrete hollow slab beam bridges. Engineering Structures, vol. 333, p. 120128. ISSN: 0141-0296, https://doi.org/10.1016/j.engstruct.2025.120128